The Journal of Organic Chemistry

Article

Influence of intramolecular charge transfer and nuclear quantum effects on intramolecular hydrogen bonds in azopyrimidines

Katerina Bartova, Lucie #echová, Eliska Prochazkova, Ondrej Socha, Zlatko Janeba, and Martin Dracinsky

J. Org. Chem., **Just Accepted Manuscript** • DOI: 10.1021/acs.joc.7b01810 • Publication Date (Web): 22 Aug 2017

ACS Publications

The Journal of Organic Chemistry is published by the American Chemical Society. 1155 Sixteenth Street N.W., Washington, DC 20036

Influence of intramolecular charge transfer and nuclear quantum effects on intramolecular hydrogen bonds in azopyrimidines

Kateřina Bártová,[†,‡] Lucie Čechová,[†,§] Eliška Procházková,[†] Ondřej Socha,[†] Zlatko Janeba,[†] Martin Dračínský[*,†]

[†]*Institute of Organic Chemistry and Biochemistry, Academy of Sciences of the Czech Republic, Flemingovo nam. 2, 166 10, Prague, Czech Republic*

[‡]*Faculty of Science, Charles University, Prague, Czech Republic*

[§]*Department of Chemistry of Natural Compounds, University of Chemistry and Technology Prague, Technická 5, 166 28 Prague, Czech Republic*

E-mail: dracinsky@uochb.cas.cz

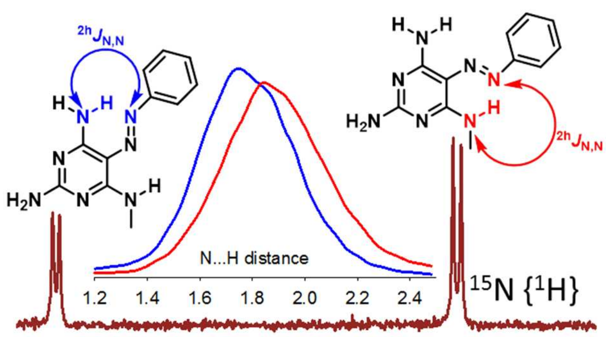

Abstract

Intramolecular hydrogen bonds (IMHBs) in 5-azopyrimidines are investigated by NMR spectroscopy and DFT computations that involve nuclear quantum effects. A series of substituted 5-phenylazopyrimidines with one or two hydrogen bond donors able to form IMHBs with the azo group is prepared by azo coupling. The barrier of interconversion between two rotamers of the compounds with two possible IMHBs is determined by variable temperature NMR spectroscopy and it is demonstrated that the barrier is significantly affected by intramolecular charge transfer. Through-hydrogen-bond scalar coupling is investigated in ^{15}N labelled compounds and the stability of the IMHBs is correlated with experimental NMR parameters and rationalized by path integral molecular dynamics simulations that involve nuclear quantum effects. Detailed information on the hydrogen bond geometry upon hydrogen-to-deuterium isotope exchange is obtained from a comparison of experimental and calculated NMR data.

Introduction

Hydrogen bonding is an enormously important and fascinating type of weak bonding that is crucial, for example, for maintaining the shape and function of proteins and nucleic acids.[1-2] However, despite its ubiquitous involvement in biomolecular processes, the detailed understanding of hydrogen bonding in terms of energies, geometric preferences and dynamics is still rather limited.[3] The biggest obstacle in hydrogen bond investigation stems from the fact that common experimental techniques for structural analysis cannot provide hydrogen atom positions with high precision. A prominent example is X-ray crystallography, which is the most widely used technique for determination of structures with atomic resolution, but hydrogen atoms are very difficult to characterize by this technique. Furthermore, hydrogen atoms may also be problematic for common computational methods, because nuclear quantum effects (NQEs), which may be important for light hydrogen nuclei, are not commonly involved in the calculations.

Intramolecular hydrogen bonds (IMHBs) affect molecular properties significantly; for example, molecules become more lipophilic and may exhibit enhanced membrane permeability upon the formation of IMHBs.[4] Molecules containing pseudoring formed by an IMHB have been proposed as bioisosteres of several biologically important molecules and it has been proven that six-membered hydrogen bonded pseudorings effectively mimic an aromatic ring.[5-11] Exceptionally stable IMHBs have recently been observed in polysubstituted 5-nitrosopyrimidine derivatives.[12-14] When two hydrogen bond donors were in the neighboring positions to the nitroso group, two stable rotamers of the nitroso group were observed and even separated in several cases.[15] The extraordinary stability of hydrogen bonds in these systems has been explained in terms of resonance-assisted hydrogen bonding (RAHB)[16-19] and intramolecular charge transfer (push–pull interactions).[20]

NMR spectroscopy is one of the most powerful tools to study the strength and geometry of hydrogen bonds, because all observable NMR parameters are affected by the formation of hydrogen bonds.[21] A direct evidence of the formation of a hydrogen bond can be obtained, for example, by the observation of a scalar coupling across the hydrogen bonds (${}^{h}J$), allowing simultaneous identification of hydrogen-bond donor and acceptor.[22] Since their first observation in 1998,[23-24] scalar interactions across hydrogen bonds have become an important tool for the structural elucidation of biological macromolecules.[3, 25-27]

Here, we present the results of our synthetic, NMR and computational study of substituted 5-phenylazopyrimidines with one (**1a**–**1c**) and with two (**2a**-**2c**) hydrogen bond donors in positions 4 and 6 (Figure 1). These compounds can form two different six-membered pseudorings with IMHBs. We demonstrate that the nature of the substituents has a large effect on the stability of the two forms of the molecules. Furthermore, ^{15}N labelling of the compounds allowed us determination of through-hydrogen-bond NMR coupling constants, which are correlated to the hydrogen bond strengths. A combination of experimental NMR data with path integral molecular dynamics (PIMD) simulations, that involve NQEs, is shown to provide intimate details about the IMHBs in these systems.

5-Azopyrimidine nucleosides with the same structural motif as the molecules investigated here have recently been suggested as nucleodyes – visibly colored nucleoside analogs with potential application in studying nucleic acids and their cellular interactions.[28] 5-Azopyrimidines have also been proposed as prodrugs of pyrimidine derivatives with antioxidant activity.[29] Generally, azocompounds have found multitude of applications ranging from synthetic chemistry to medicine and nanorobotics.[30-45]

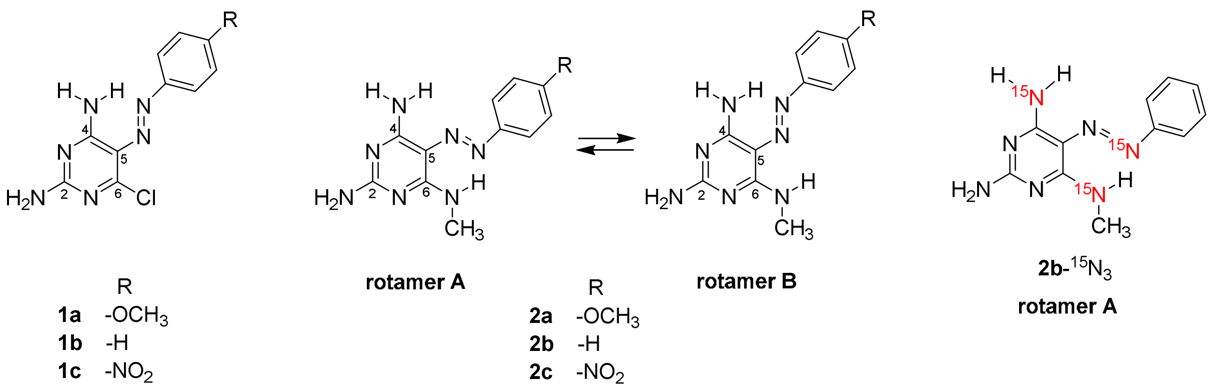

Figure 1. The structure of the studied compounds.

Results and Discussion

Synthesis

The key reaction step in the synthesis of the target compounds **1** and **2** is azo coupling between properly substituted pyrimidine and aromatic diazonium salt formed from aniline bearing a substituent in *para* position of the phenyl ring (*p*-NO_2, *p*-OMe). Thus, azo coupling of 2-amino-4,6-dihydroxypyrimidine (**3**) with benzenediazonium chlorides **4a**, **4b** and **4b**-$^{15}N_1$ (Scheme 1) gave azo compounds **5a**, **5b** and **5b**-$^{15}N_1$, respectively, as solids that precipitated from the reaction mixtures. The products **5** were chlorinated with Vilsmeier-Haack-Arnold reagent to obtain 4,6-dichloropyrimidine derivatives **6**. The conventional heating of compounds **6** with ethanolic ammonia or methanolic ^{15}N ammonia solutions afforded compounds **1** and subsequent heating of compounds **1** with ethanolic methylamine solution or with ^{15}N methylamine hydrochloride in isopropanol under microwave conditions gave desired products **2** (Scheme 1). Similarly, azo coupling of 2,4-diamino-6-chloropyrimidine (**7**, Scheme 1) with *p*-nitrobenzenediazonium chloride **4c** led to the formation of azo compound **1c**, which upon treatment with ethanolic methylamine solution afforded final derivative **2c**. Purification of final azo compounds **1** and **2** was quite laborious and multiple reverse phase chromatographies were necessary to obtain pure products.

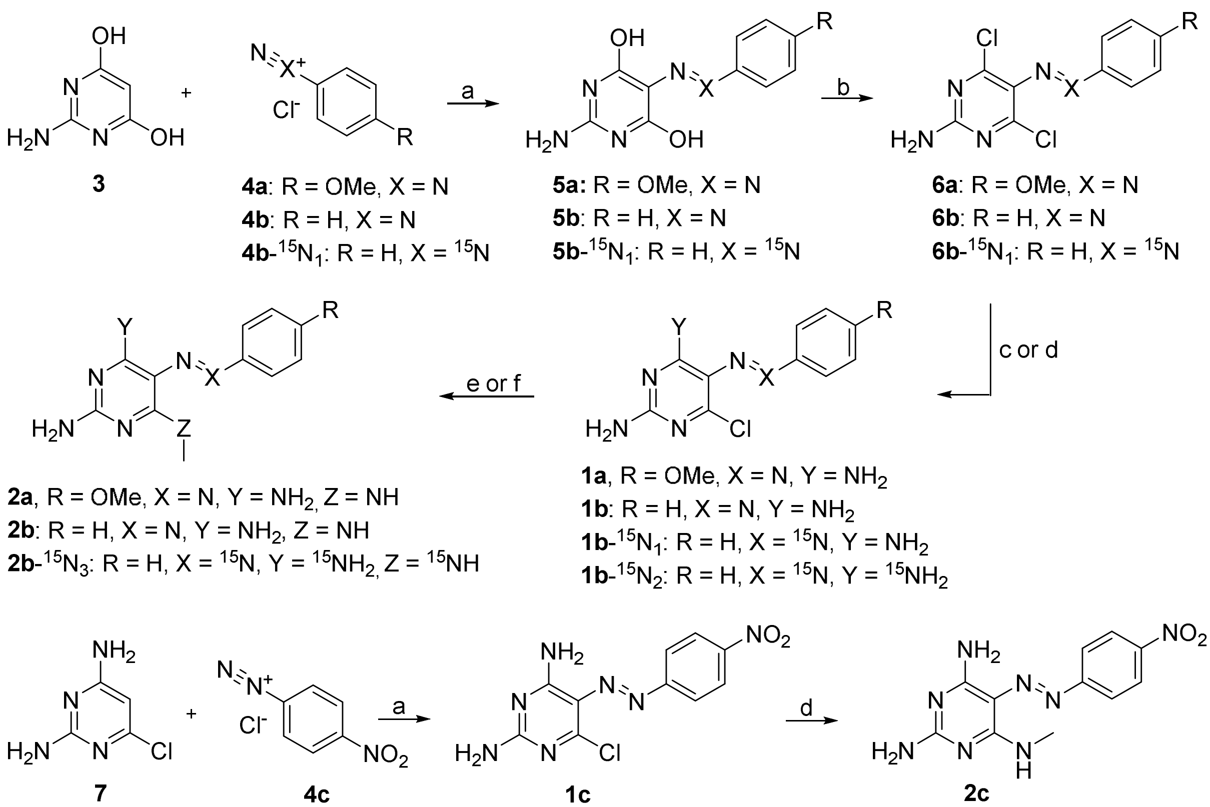

Scheme 1. Synthesis of target azo compounds **1** and **2**.

Reagents and conditions: (a) acetic buffer (pH 7), rt, overnight; (b) Vilsmeier-Haack-Arnold reagent, $CHCl_3$, reflux, 1–3 h, 59–78 %; (c) NH_3 (2M ethanolic solution), 60 °C (conventional heating), 1–12 h, 20–60 %; (d) ^{15}N NH_3 (methanolic solution), 60 °C (conventional heating), 12 h, 33 %; (e) methylamine (33% ethanolic solution), 150 °C (MW conditions), 10–30 min, 27–40 %; (f) ^{15}N methylamine hydrochloride, *i*PrOH, 150 °C (MW conditions), 1 h, 20 %.

NMR Spectroscopy

One set of signals is observed in NMR spectra of chloro derivatives **1a**–**1c**. The formation of a six-membered pseudoring with IMHB can be inferred from the chemical shifts of protons in the NH_2 group in position 4; the two amino hydrogen atoms are not equivalent and the hydrogen atom involved in IMHB resonates at higher chemical shift values (1–1.2 ppm downfield than the other hydrogen atom).

Compounds **2a**–**2c** with two hydrogen bond donors in positions 4 and 6 may form two stable IMHBs (rotamer A and rotamer B, Figure 1), which can lead to observation of two sets of signals in NMR spectra. However, variable temperature NMR experiments with compounds **2a**–**2c** revealed remarkable differences in the interconversion barriers between these two rotamers. In ^{1}H NMR spectrum of compound **2c** with nitro substituent, two sets of signals are well resolved at room temperature and, for example, the coalescence of the methyl signals (Figure 2) is observed at 310 K. On the other hand, the coalescence of this signal in the spectra of compounds **2b** and **2a** is observed at lower temperature (260 K and 240 K, respectively). The rotational barriers (barriers of interconversion between rotamer A and B) were estimated from lineshape analysis of the variable temperature proton spectra and from the coalescence temperature (Table 1 and Table S1 in Supporting Information). The observed rotamer ratio is almost independent on the substituent in the phenyl ring and temperature. Rotamer A with the azo group heading towards the methylamino group is always more stable and the rotamer ratio is ca 6:4. For comparison, we have also prepared compound **2d** analogous to **2c** with the nitro substituent in *meta* position to the azo group and determined the interconversion barrier (SI). The push–pull interaction is evidently suppressed in this compound.

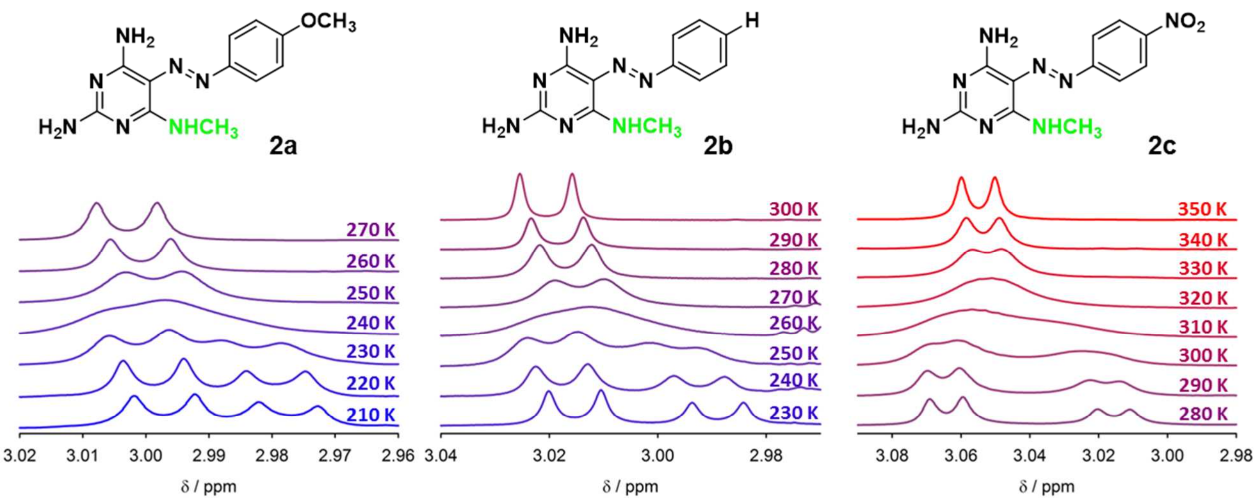

Figure 2. Variable temperature ^{1}H NMR spectra of compounds **2a**–**2c**. Only the region with methyl signals of the methylamino group is depicted.

Table 1. Experimental and calculated interconversion barriers (kcal/mol) between two rotamers of compounds **2a**–**2c**.

Compound	Substituent	Coalescence T / K^{a}	$\Delta G^{\#}$(exp)^{b}	$\Delta G^{\#}$(calc)
2a	*p*-OMe	240	12.5±0.3	14.7
2b	–	260	13.4±0.3	15.9
2c	*p*-NO_2	320	16.2±0.3	20.6

^{a}Coalescence of methylamino CH_3 signals; ^{b}calculated at coalescence temperature using the equation $k = 2.22*\Delta\nu$, where k is the rate constant and $\Delta\nu$ is the difference of resonance frequency of methyl hydrogens in rotamer A and B, full details are given in Table S1 in the SI.

The differences in the heights of the rotational barriers in compounds **2a**–**2c** may be caused either by differences in the stability of the IMHB induced by the substituents or by increased bond order of the C5–N bond caused by intramolecular charge transfer (push–pull interaction). The influence of the substituent on the hydrogen bond strength might be deduced from the changes of chemical shifts of amino and methylamino NH protons. The contribution of the electronic nature of the *para*-substituent to magnetic shielding of amino hydrogens in position 4 and methylamino hydrogen in position 6 should be identical, because it is transferred via the same structural fragment. Chemical shifts of the (methyl)amino NH protons in rotamer A of compounds **2a**–**2c** measured at 210 K depend on the substituent, but those involved and not involved in IMHB change evenly (SI, Table S2). Therefore, the hydrogen bond strength is probably not affected by the substituent in the phenyl ring.

Two sets of signals with 6:4 ratio corresponding to rotamers A and B can also be observed in ^{15}N NMR spectrum of compound **2b-**$^{15}N_3$. The signal assignment was done with the help of compounds **1b-**$^{15}N_1$ and **1b-**$^{15}N_2$ with one and two ^{15}N labels, respectively. Azo nitrogen (Figure S1, SI) in proton decoupled ^{15}N spectrum appears as a doublet close to 400 ppm for both rotamers; the splitting of the signal is caused by through-hydrogen bond interaction ($^{2h}J_{N,N}$) with the ^{15}N amino nitrogen in position 6 or 4. These amino nitrogens are observed in the region of 70–95 ppm. The signals of amino nitrogen atoms involved in the hydrogen bond appear at higher chemical shifts (close to 90 ppm) and are split by the above mentioned through-hydrogen bond coupling in proton-decoupled spectra (Figure 3). Further splitting to triplet (NH_2 group, rotamer B) or doublet (NHMe group, rotamer A) is observable in proton-coupled spectra due to one-bond $^{1}J_{N–H}$ interaction. The signals of nitrogen atoms not involved in the hydrogen bond appear at lower chemical shifts (ca 15 ppm upfield). Hydrogen bonding also influences the $^{1}J_{N–H}$ coupling constant between the hydrogen-bond donor and the hydrogen atom. It has been documented that strong hydrogen bonding results in a decrease of the $^{1}J_{N\text{–}H}$ coupling constant across the corresponding N–H covalent bond.[26, 46] Indeed, slightly smaller $^{1}J_{N\text{–}H}$ interaction is observed for amino groups involved in hydrogen bonds, i.e. in NH_2 group of rotamer B and NHMe group in rotamer A.

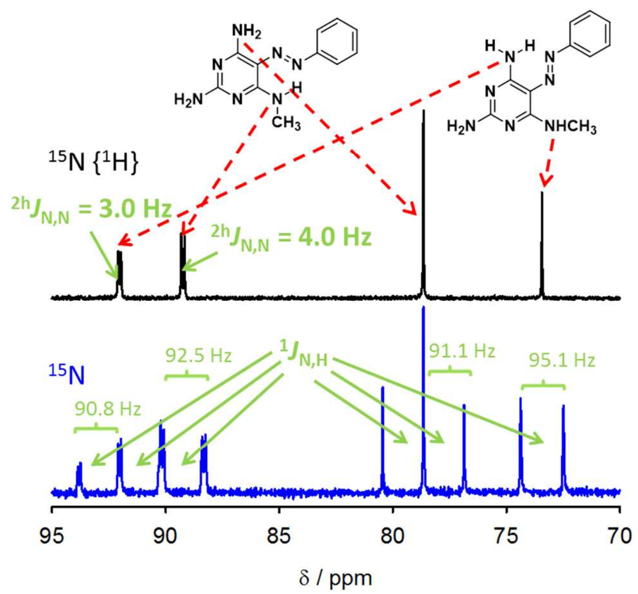

Figure 3. Amino and methylamino region of proton-coupled (blue) and proton-decoupled (black) ^{15}N NMR spectra of compound **2b**-$^{15}N_3$.

Through-hydrogen-bond coupling may also be detected between the amino/methylamino hydrogen atom and the azo nitrogen atom. This interaction leads to observation of through-hydrogen bond cross-peaks in H,N-HMBC spectra of compound **2b**-$^{15}N_3$ and to splitting of the NH signal in ^{1}H NMR spectrum (Figure 4). All relevant H–N and N–N couplings observed in compound **2b**-$^{15}N_3$ are summarized in Figure 5. The $^{1h}J_{N,H}$ and $^{2h}J_{N,N}$ through-hydrogen bond couplings have values typically found in systems with N–H···N hydrogen bonds.[3] It can be seen that both observable through-hydrogen-bond couplings ($^{1h}J_{N,H}$ and $^{2h}J_{N,N}$) are larger in rotamer A, which corresponds to stronger hydrogen bond interaction of the methylamino group leading also to higher relative concentration of rotamer A.

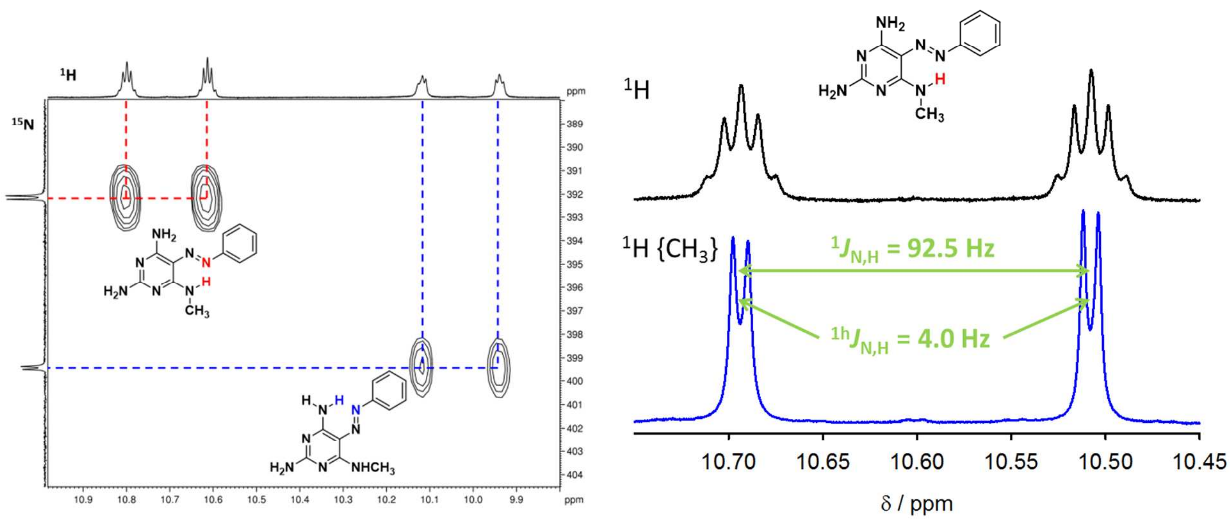

Figure 4. Left: part of H,N-HMBC spectrum of compound **2b**-$^{15}N_3$ measured at 230K with through-hydrogen bond interactions. Right: Methylamino-hydrogen region of proton NMR spectrum of compound **2b**-$^{15}N_3$ acquired at 230 K (black) and the same spectrum with selective homodecoupling of the CH_3 protons (blue).

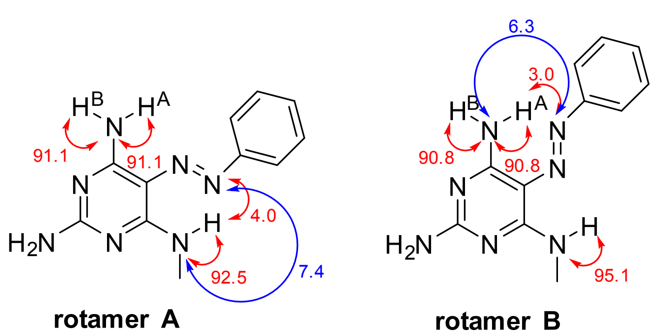

Figure 5. Selected N–H (red) and N–N scalar coupling constant values observed in both rotamers of compound **2b**-$^{15}N_3$.

It has recently been shown that hydrogen bonding interactions in RAHBs are closely related to nuclear quantum effects (NQEs), particularly to the delocalization of hydrogen nucleus.[19] One of the consequences of NQEs is the effect of deuterium isotope substitution on the hydrogen bond properties. Therefore, we prepared compound **2b**-$^{15}N_3$ with ca 1:1 hydrogen to deuterium isotope exchange of the amino and methylamino hydrogens and acquired ^{15}N NMR spectra. The effect of deuteration on NMR spectra is twofold: first, ^{15}N signals are shifted due to deuterium isotope shift (Table 2) and second, the value of $^{2h}J_{N,N}$ through-hydrogen bond coupling in rotamer A is slightly reduced (7.4 → 7.3 Hz).

Table 2. Experimental deuterium isotope induced changes of nitrogen chemical shifts (ppm) and through-hydrogen-bond coupling (Hz) in compound **2b**-$^{15}N_3$ and calculated isotope-induced changes of N–H bond distances (Å).

	Rotamer A		Rotamer B		
	$\Delta\delta$ / ΔJ^a	Δd(N6–H)^b	$\Delta\delta$ / ΔJ^a	Δd(N6–H)^b	Δd(N4–H^A)^b
N6	1.05	0.007	0.62	0.004	
N4	0.55		~0.7^c		
N-azo	–0.74	0.006	~–0.5^c		0.005
$^{2h}J_{N6,N\text{-azo}}$	0.1	0.008			

^{a}Calculated as the difference between protonated and deuterated compound, i.e. positive value means upfield shift; ^{b}calculated from the experimental deuterium-induced ^{15}N chemical shift and $^{2h}J_{N6,N\text{-azo}}$ changes and DFT calculated dependence of these NMR parameters on N–H bond distance; ^{c}signal broadening due to 0, 1 or 2 hydrogen atom exchange in NH_2 group.

Calculations

To better understand the intramolecular hydrogen bonding and its influence on the structure and properties of the studied molecules, we performed a number of density functional theory (DFT) calculations. First, we optimized the geometries of both rotamers of compounds **2a**–**2c** and calculated magnetic shielding of the nuclei and scalar coupling values. Excellent correlation between the calculated shielding values and experimental chemical shifts was observed (SI, Figure S2), which confirmed our signal assignment. The calculated coupling constant values reproduce well the trends observed in compound **2b**-$^{15}N_3$, i.e. $^{1h}J_{H,N}$ and $^{2h}J_{N,N}$ through-hydrogen bond couplings are larger in rotamer A of compound **2b** and $^{1}J_{N–H}$ coupling constants decrease upon hydrogen bond formation (Table S3). Furthermore, the calculations revealed that the through-hydrogen bond couplings are almost independent on the substitution on the phenyl ring. This confirms our conclusion, inferred from experimental proton chemical shifts, that the substitution does not affect the hydrogen bond strength.

The calculated barriers of rotamer interconversion reproduce the trends observed by variable-temperature NMR experiments, i.e. the highest barrier is in compound **2c** followed by **2b** and **2a**. Given that the hydrogen bond strength is similar in all three compounds, the differences in rotamer interconversion barriers must be caused by push-pull interactions of the substituents. For example, electron-donating substituents in the pyrimidine ring of compound **2c** push electron density towards the electron-withdrawing nitro substituent in the phenyl ring. This is well reflected in the calculated electrostatic potential plots (Figure S3) bond distances in compounds **2a**–**2c** (Table S4), where the C5–N distance is significantly smaller in compound **2c** (1.348 Å) than in compound **2b** (1.365 Å) and **2a** (1.370 Å). Smaller bond distance corresponds to higher bond order and hence to higher rotational barrier.

To estimate the geometry changes in the IMHBs upon hydrogen-to-deuterium isotope exchange, the experimental isotope-induced changes of nitrogen chemical shifts and $^{2h}J_{N,N}$

coupling were compared with a DFT calculated dependence of nitrogen shieldings and through-hydrogen-bond couplings on the 6N–H and 4N–H bond distances. The calculations revealed that lengthening of N–H distance leads to smaller shielding of the NH nitrogen atom, larger shielding of the hydrogen-bonded azo nitrogen and larger through-hydrogen-bond couplings $^{1h}J_{N,H}$ and $^{2h}J_{N,N}$.The comparison of the calculated distance dependence of shieldings and couplings with experimental isotope-exchange induced changes was used to estimate average deuterium-induced bond-length shortening of 0.006–0.008 Å in the case of N6-H in rotamer A (involved in IMHB) and to a smaller shortening of N6–H in rotamer B (not involved in IMHB) and of N4–H in rotamer B (involved in a weaker IMHB, see Table 2).

It has recently been demonstrated that an incorporation of NQEs is important for an accurate prediction of hydrogen bond properties, because hydrogen atom possess the lightest nucleus and effects, such as tunneling or delocalization of nuclear positions, become more important than for heavier nuclei.[19, 47-51] One way of incorporation of NQEs into quantum-chemical calculations is path integral molecular dynamics (PIMD). PIMD simulations use a decomposition of nuclei into a set of “beads” connected with harmonic oscillators; the force constant of the oscillator depends on the nuclear mass and temperature. Light nuclei and low temperatures lead to more delocalized nuclei.

We applied PIMD simulations to compounds **1a**–**1c** and to both rotamers of compound **2b** and we analyzed the simulations by plotting probability distributions of bond distances between atoms involved in the IMHBs. The probability distribution of N–H distances in compounds **1a**–**1c** shows that the amino N–H bond involved in the IMHB is longer and the probability distribution of this N–H distance is broader (the hydrogen is more delocalized) than for the N–H bond not involved in the IMHB. The N–H and H···N distances are almost identical for all three compounds **1a**–**1c** (SI, Figure S4), which confirms our conclusion that the substituent on the phenyl ring does not affect the hydrogen bond strength.

On the other hand, the probability distributions found for compound **2b** depend significantly on the conformation (rotamer A or B, see Figure 6). The 6N–H of rotamer A (involved in IMHB) probability distribution is slightly broader and shifted towards higher distances than the 4N–H^A of rotamer B (also involved in IMHB) distribution. The distance between hydrogen bond donor and the hydrogen atom has been correlated to hydrogen bond strength.[52] These probability distributions thus reflect the stability of the two rotamers: rotamer A is more abundant because the hydrogen atom in the IMHB is more delocalized and hence, the hydrogen bond in this rotamer is more stable. The distance probabilities of N–H bonds not involved in IMHBs are significantly narrower and shifted to shorter values. Significantly narrower distribution is also observed for N–D distances in deuterated compound **2b**. Similar information about the geometry of the IMHBs can be obtained from probability distributions of distances between the hydrogen atom and the hydrogen bond acceptor (azo nitrogen). In rotamer A, the H···N distance probability is significantly shorter than in rotamer B and deuteration leads to lengthening of the H···N distance (Figure S5). All relevant average distances between atoms involved in the IMHBs obtained from the PIMD simulations are listed in the SI (Table S7).

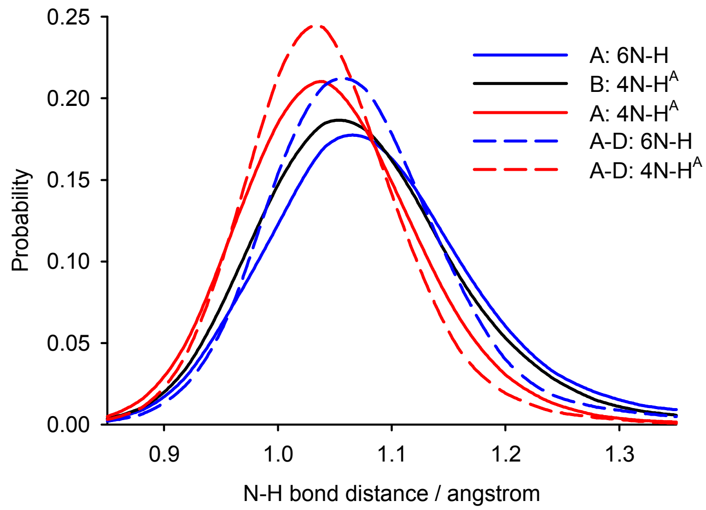

Figure 6. Probability distribution of selected N–H distances in rotamers A and B of compound **2b** and of deuterated rotamer A (A-D) found in PIMD simulations.

Conclusions

Intramolecular hydrogen bonds in substituted 5-phenylazopyrimidines were studied by NMR spectroscopy and DFT calculations. Both experimental chemical shifts, and computed N–H bond distances and through-hydrogen-bond scalar couplings indicate that the hydrogen-bond strength is not affected by the substitution in *para* position of the phenyl ring. The substituents have, however, a large effect on the C5–N rotational barrier, which was explained in terms of push–pull interactions of the substituents. Electron-donating substituents (amino groups) in the pyrimidine ring push electron density through the azo nitrogens to the phenyl ring. This intramolecular charge transfer is more effective when an electron-accepting (nitro) substituent is in *para* position of the phenyl ring. The intramolecular charge transfer increases the C5–N bond order and, hence, also the C5–N rotational barrier.

In compounds with two hydrogen-bond donors in neighboring positions to the azo group, two different IMHBs can exist, both leading to the formation of a six-membered pseudo ring. The formation of the IMHBs in these two structures was confirmed, for example, by the observation of through-hydrogen-bond scalar couplings. Rotamer A with the pseudoring formed with the methylamino group was more stable than rotamer B in all studied compounds. Higher stability of rotamer A is reflected in larger shielding of the hydrogen-bond acceptor (azo-nitrogen) and larger through-hydrogen-bond couplings in this rotamer. Higher stability of the IMHB in rotamer A was also confirmed by PIMD simulations, where larger delocalization of the hydrogen atom in the IMHB in rotamer A was observed. This larger delocalization of the hydrogen atom also leads to larger deuterium-isotope-induced changes of nitrogen chemical shifts, which were confirmed experimentally.

The potential applications of the studied compounds range from biocompatible azodyes to orthogonal molecular switches with switching either the IMHB (rotamer A or B) or the *cis*/*trans* isomers of the azo group, which is a widely exploited type of isomerism in many applications. The work presented here demonstrates that fine tuning of the switching barrier between the rotamers A and B is possible by introducing proper substituents in the phenyl ring. These substituents do not influence the hydrogen bond strengths, which are controlled by the nature of the hydrogen bond donors. Relative strengths of the IMHBs can easily be determined by NMR spectroscopy. The combination of experimental NMR data with DFT calculations enables to obtain intimate details about IMHBs, such as the changes of hydrogen bond geometry upon hydrogen-to-deuterium isotope exchange.

EXPERIMENTAL SECTION

General. Instrumentation and calculations.

Unless otherwise stated, solvents were evaporated at 40 °C/2 kPa, and the compounds were dried over P_2O_5 at 2 kPa. Analytical TLC was performed on silica gel pre-coated aluminium plates with fluorescent indicator (Merck 5554, 60 F_{254}). Spots were visualized with UV light (254 nm). Flash reversed-phase chromatography was carrried out on CombiFlash® Rf+ (TELEDYNE ISCO) with RediSep RF Gold® C18 Aq column (50 g, 20-40 μm, TELEDYNE ISCO). Mass spectra were measured on a Q-Tof micro (Waters) and HR MS were taken on a LTQ Orbitrap XL (Thermo Fisher Scientific) spectrometer. Melting points were measured on a Stuart SMP3Melting Point Apparatus

The microwave-assisted reactions were carried out in CEM Discover (Explorer) microwave aparatus, 24-position system for 10-mL vessels sealed with Teflon septum. It was operated at a frequency of 2.45 GHz with continuous irradiation power from 0 to 300W. The solutions were steadily stirred during the reaction. The temperature was measured with an IR sensor on the outer of the process vessel. The vials were cooled to ambient temperature with gas jet cooling system. The pressure was measured with an inboard CEM Explorer pressure control system (0-21 bar).

^{1}H and ^{13}C NMR spectra were recorded on a 400, 500 and/or 600 MHz NMR spectrometer (^{1}H at 400 MHz and ^{13}C at 100.6 MHz, or ^{1}H at 500 MHz, ^{13}C at 125.7 MHz and ^{15}N at 50.7 MHz, or ^{1}H at 600.1 MHz and ^{13}C at 150.9 MHz) in DMSO-d_6 (referenced to the solvent signal δ = 2.50 and 39.70 ppm, respectively) and DMF-d_7 (referenced to the solvent signal δ = 2.75 (^{1}H), 104.9 (^{15}N) and 163.15 ppm (^{13}C), respectively). Complete signal assignment is based on heteronuclear correlation experiments HSQC and HMBC. The ^{15}N chemical shifts were determined using 1D experiment with direct detection of nitrogens and gated decoupling of hydrogen nuclei. For the assignment of ^{15}N signals based on coupling with directly attached hydrogen atoms, proton coupled nitrogen NMR spectra were also measured. Chemical shifts (δ) are in ppm and coupling constants (*J*) in Hz. Partly deuterated compound **2b**-$^{15}N_3$ was prepared by adding a drop of D_2O into the DMF solution of the compound and evaporating to dryness under reduced pressure.

The studied structures were subjected to geometry optimization at DFT level, using B3LYP functional,[53-54] standard 6-31+G(d,p) basis set and polarizable continuum model used for implicit DMF solvation.[55-56] NMR shielding values and scalar coupling constants were calculated for the optimized structures. The Gaussian09 program package was used throughout this study.[57] The QST3 optimization method[58-59] was applied in the search for the transition state structures of the rotamer interconversion, that is the structures of the reactant, product, and estimated transition state were used as input for the TS search. The vibrational frequencies and free energies were calculated for all of the optimized structures, and the stationary-point character (a minimum or a first-order saddle point) was thus confirmed.

The dependence of nitrogen shieldings and through-hydrogen-bond couplings on the 6N–H and 4N–H bond distances was calculated by manually adjusting the bond distance in the range 0.9–1.3 Å (with a 0.1 Å step). The calculated distance dependence of the shielding and coupling values was fitted to a straight line.

Path integral molecular dynamics (PIMD) simulations were run in the CASTEP program,[60] which is a DFT-based code, using an *NVT* ensemble maintained at a constant temperature of 300 K using a Langevin thermostat, a 0.5 fs integration time step, simulation length of 5 ps, ultrasoft pseudopotentials,[61] a planewave cutoff energy of 300 eV, and with integrals taken over the Brillouin zone using a Monkhorst-Pack[62] grid of a minimum *k*-point sampling of 0.1 $Å^{-1}$. Electron-correlation effects were modelled using the generalized gradient approximation of

Perdew, Burke, and Ernzerhof.[63] The atomic positions were optimized at the same computational level prior to the PIMD runs. Compounds **1a**–**1c** and both rotamers of compound **2b** were modelled as isolated molecules in a cubic periodic box of 16 x 16 x 16 Å^3. The path integral was used on top of the DFT-MD simulations, with a Trotter decomposition of all nuclei into $P = 16$ beads. For the evaluation of deuterium isotope effects, new PIMD simulations were performed with the mass of all exchangeable protons (all N–H protons) adjusted to the mass of deuterium. Probability distributions of the N4–H and N6–H bond distances were plotted with 0.04 Å step. The PIMD distance probabilities were determined independently for all 16 replicas and then averaged.

General procedure A. Substituted aniline (1.2 eq) was dissolved in 1M HCl (5 mL), the solution was cooled to 0 °C and sodium nitrite (1.3 eq) was added. The reaction mixture was stirred for 30 min at 0 °C. The solution of formed diazonium salt **4** was then added dropwise to a solution of 2-amino-4,6-dihydroxypyrimidine (**3**, 1 eq) in acetic buffer and the mixture was stirred overnight. Precipitated solid was filtreted and dried to obtain 4,6-dihydroxypyrimidine intermediates **5**. Compounds **5** were consequently treated with Vilsmeier-Haack-Arnold reagent (4.0 eq) in $CHCl_3$ (40 mL) at reflux. The solvent was evaporated to dryness. The formed 2-(dimethylamino)methylene)amino substituted pyrimidine was dissolved in water (40 mL) with catalytic amount of concentrated HCl. The reaction mixture was stirred overnight and precipitated solid was filtered and dried. Reversed-phase flash chromatography (MeOH/H_2O, 0-100 %) gave desired 4,6-dichloropyrimidine products **6**.

4,6-Dichloro-5-((4-methoxyphenyl)diazenyl)pyrimidin-2-amine (**6a**). Treatment of *p*-anisinide (145 mg, 1.2 mmol) with sodium nitrite (88 mg, 1.3 mmol) by procedure A afforded diazonium salt **4a**, which reacted with 2-amino-4,6-dihydroxypyrimidine (**3**, 127 mg, 1 mmol) to give 2-amino-5-((4-methoxyphenyl)diazenyl)pyrimidine-4,6-diol (**5a**). Treatment of **5a** (1 g, 3.8 mmol) with Vilsmeier-Haack-Arnold reagent (1.946 g, 15.2 mmol) for 3 h gave **6a** (940 mg, 78 %) as an orange solid, m. p. 220–230 °C. ^{1}H NMR (DMSO-d_6, 298 K): 7.97 (2H, bs, NH_2), 7.82 (2H, m, H2'), 7.14 (2H, m, H3'); ^{13}C NMR (DMSO-d_6, 298 K): 162.7 (C4'), 160.3 (C2), 154.9 (C4 and C6), 146.6 (C1'), 130.5 (C5), 124.7 (C2'), 114.9 (C3'), 55.9 (OCH_3); ESI MS, *m/z* (%): 298.1 $[M + H]^+$; HRMS (ESI) calcd for $C_{11}H_{10}Cl_2N_5O$ $[M + H]^+$ 298.0257, found 298.0257.

4,6-Dichloro-5-(phenyldiazenyl)pyrimidin-2-amine (**6b**). Treatment of aniline (0.2 mL, 2.4 mmol) with sodium nitrite (176 mg, 2.6 mmol) by procedure A gave diazonium salt **4b**, which reacted with 2-amino-4,6-dihyroxypyrimidine (**3**, 254 mg, 2 mmol) to give 2-amino-5-(phenyldiazenyl)pyrimidine-4,6-diol (**5b**). Treatment of **5b** (100 mg, 0.4 mmol) with Vilsmeier-Haack-Arnold reagent (205 mg, 1.6 mmol) for 1h gave **6b** (73 mg, 68 %) as a red solid, m. p . 160-173 °C. ^{1}H NMR (DMSO-d_6): 8.10 (2H, bs, NH_2), 7.82 (2H, m, H2'), 7.63-7.56 (3H, m, H3' and H4'); ^{13}C NMR (DMSO-d_6): 160.5 (C2), 155.5 (C4 and C6), 152.3 (C1'), 132.1 (C4'), 130.3 (C5), 129.8 (C3'), 122.5 (C2'); ESI MS, *m/z* (%): 268.0 $[M + H]^+$; HRMS (ESI) calcd for $C_{10}H_8Cl_2N_5$ $[M + H]^+$ 268.0151, found 268.0149.

4,6-Dichloro-5-(phenyldiazenyl-2-^{15}N)pyrimidin-2-amine (**6b-^{15}N$_1$**). Treatment of aniline-^{15}N (0.12 mL, 1.2 mmol) with sodium nitrite (74 mg, 1.3 mmol) by procedure A gave diazonium salt **4b-^{15}N$_1$**, which reacts with 2-amino-4,6-dihydroxypyrimidine (**3**, 127 mg, 1 mmol) to give 2-amino-5-(phenyldiazenyl-2-^{15}N)pyrimidine-4,6-diol (**5b-^{15}N$_1$**). Treatment of **5b-^{15}N$_1$** (100 mg, 0.6 mmol) with Vilsmeier-Haack-Arnold reagent (307 mg, 2.4 mmol) for gave **6b-^{15}N$_1$** (95 mg, 59 %) as red solid. ^{1}H NMR (DMSO-d_6): 8.10 (2H, bs, NH_2), 7.81 (2H, m, H2'), 7.62-7.56 (3H, m, H3’ and H4’); ^{13}C NMR (DMSO-d_6): 160.5 (C2), 155.5 (d, $J_{C\text{-}C\text{-}N\text{-}N}$ = 2.0, C4 and C6), 152.3 (d, $J_{C\text{-}N}$ = 2.5, C1’), 132.1 (C4’), 130.3 (d, $J_{C\text{-}N\text{-}N}$ = 5.2, C5), 129.8 (d, $J_{C\text{-}C\text{-}C\text{-}N}$ = 1.9, C3’), 122.5 (d, $J_{C\text{-}C\text{-}N}$ = 4.0, C2’); ESI MS, *m/z* (%): 269.0 $[M + H]^+$; HRMS (ESI) calcd for $C_{10}H_8N_4{}^{15}NCl_2$ $[M + H]^+$ 269.0122, found 269.0123.

6-Chloro-5-((4-nitrophenyl)diazenyl)pyrimidine-2,4-diamine (**1c**). Sodium nitrite (88 mg, 1.3 mmol) was added to the cooled (0 °C) solution of *p*-nitroaniline (166 mg, 1.2 mmol) in 1M HCl (5 mL) and the reaction mixture was stirred for 30 min at 0 °C to give a solution of diazonium salt **4c**. To this solution, a solution of 2,4-diamino-6-hydroxypyrimidine (**3**, 144 mg, 1 mmol) in acetic buffer was added dropwise and the reaction mixture was stirred overnight. Precipitated solid was filtered and reversed-phase flash chromatography (0-100 % MeOH in water) gave **1c** (188 mg, 64 %) as an orange solid, m. p. > 300 °C. ^{1}H NMR (DMSO-d_6): 9.40 (1H, d, J_{GEM}= 3.3, 4-NH^a), 8.41 (1H, d, J_{GEM}= 3.3, 4-NH^b), 8.35 (2H, m, H3’), 7.98 (2H, m, H2’), 7.74 (1H, bs, 2-NH^b), 7.55 (1H, bs, 2-NH^a); ^{13}C NMR (DMSO-d_6): 166.0 (C6), 161.1 (C2), 156.5 (C1’), 156.0 (C4), 146.8 (C4’), 125.2 (C3’), 122.3 (C2’), 119.9 (C5); ESI MS, *m/z* (%): 294.1 $[M + H]^+$; HRMS (ESI) calcd for $C_{10}H_9ClN_7O_2$ $[M + H]^+$ 294.0501, found 294.0503.

General procedure B. Starting 4,6-dichloropyrimidine derivative **6** was dissolved in ammonia (2.5 M ethanolic solution) and the reaction mixture was heated at 60 °C. Water (50 mL) was added and obtained solution was extracted with EtOAc (3 x 40 mL). Organic layers were collected, dried over $MgSO_4$ and filtered. Solution was evaporated under vacuum and pure product was obtained by reversed-phase flash chromatography (0-100 % MeOH in water).

6-Chloro-5-((4-methoxyphenyl)diazenyl)pyrimidine-2,4-diamine (**1a**). Treatment of **6a** (50 mg, 0.2 mmol) with ammonia (10 mL) for 4 h by procedure B gave **1a** (10 mg, 20 %) as a yellow solid, m. p. 250–253 °C. ^{1}H NMR (DMSO-d_6): 9.21 (1H, d, J_{GEM}= 3.7, 6-NH^{a}), 7.98 (1H, d, J_{GEM}= 3.7, 6-NH^{b}), 7.77 (2H, m, H2'), 7.30 and 7.15 (2H, bs, 2-NH$_2$), 7.06 (2H, m, 3'), 3.82 (3H, s, 4'-O-CH$_3$); ^{13}C NMR (DMSO-d_6): 136.8 (C4), 161.1 (C2), 160.6 (C4'), 156.2 (C6), 145.7 (C1'), 123.2 (C2'), 118.5 (C5), 114.7 (C3'), 55. 7 (OCH$_3$); ESI MS, *m/z* (%): 279.1 [M + H]$^+$; HRMS (ESI) calcd for $C_{11}H_{12}N_6OCl$ [M + H]$^+$ 279.0756, found 279.0756.

6-Chloro-5-(phenyldiazenyl)pyrimidine-2,4-diamine (**1b**) Treatment of **6b** (50 mg, 0.2 mmol) with ammonia (10 mL) overnight by procedure B gave **1b** (30 mg, 60 %) as a yellow solid, m. p. 230–245 °C (decomp.). ^{1}H NMR (DMSO-d_6): 9.29 (1H, d, J_{GEM}= 3.6, 6-NH^{a}), 8.11 (1H, d, J_{GEM}= 3.6, 6-NH^{b}), 7.78 (2H, m, H2'), 7.51 (2H, m, H3'), 7.44 and 7.26 (2H, bs, 2-NH$_2$), 7.40 (1H, m, H4'); ^{13}C NMR (DMSO-d_6): 164.6 (C4), 161.3 (C2), 156.2 (C6), 152.5 (C1'), 129.5 (C4'), 129.4 (C3'), 121.6 (C2'), 118.8 (C5); ESI MS, *m/z* (%): 249.1 [M + H]$^+$; HRMS (ESI) calcd for $C_{10}H_{10}ClN_6$ [M + H]$^+$ 249.0650, found 249.0650.

6-Chloro-5-(phenyldiazenyl-2-^{15}N)pyrimidine-2,4-diamine (**1b-^{15}N$_1$**). Treatment of **6b-^{15}N$_1$** (100 mg, 0.4 mmol) with ammonia (10 mL) for 6 h by procedure B gave **1b-^{15}N$_1$** (60 mg, 60 %) as a yellow solid, m. p. 248–250 °C. ^{1}H NMR (DMSO-d_6, 298 K): 9.29 (1H, m, 4-NH^{A}), 8.05 (1H, d, J_{GEM} = 3.9, 4-NH^{B}), 7.77 (2H, m, H2'), 7.50 (2H, m, H3'), 7.39 (1H, m, H4'); ^{13}C NMR (DMSO-d_6, 298 K): 164.8 (d, $^{3}J_{C\text{-}N}$ = 3.1, C4), 161.4 (C2), 156.3 (C6), 152.6 (C1'), 129.8 (C4'), 129.7 (d, $^{3}J_{C\text{-}N}$ = 2.0, C3'), 121.8 (d, $^{2}J_{C\text{-}N}$ = 3.6, C2'), 118.9 (d, $^{2}J_{C\text{-}N}$ = 4.0, C5); ESI MS, *m/z* (%): 250.1 [M + H]$^+$; HRMS (ESI) calcd for $C_{10}H_{10}N_5{}^{15}NCl$ [M + H]$^+$ 250.0620, found 250.0620.

6-Chloro-5-(phenyldiazenyl-2-^{15}N)pyrimidine-2,4-diamine-^{15}N (**1b-^{15}N$_2$**). Ammonia-^{15}N (0.1 mL, 2 M methanolic solution) was added to the solution of compound **6b-^{15}N$_1$** (200 mg, 0.7 mmol) in MeOH (10 mL) and the reaction mixture was heated at 60 °C for 6 h. Water (50 mL) was added and obtained solution was extracted with EtOAc (3 x 40 mL). Organic layers were collected, dried over $MgSO_4$ and filtered. Solution was evaporated under vacuum and reversed-phase flash chromatography (0-100 % MeOH in water) gave **1b-^{15}N$_2$** (150 mg, 33 %) as a yellow solid, m. p. 234–236 °C. ^{1}H NMR (DMSO-d_6, 298.5 K): 9.30 (1H, dt, $J_{H\text{-}N}$ = 90.1, J_{GEM} = $J_{H\text{-}N}$ = 3.8, 4-NH^a), 8.12 (1H, dd, $J_{H\text{-}N}$ = 90.7, J_{GEM} = 3.9, 4-NH^b), 7.78 (2H, m, H-2'), 7.50 (2H, m, H-3'), 7.40 (1H, m, H-4'); ^{13}C NMR (DMSO-d_6, 298.5 K): 164.7 (dd, $^3J_{C\text{-}N}$ = 3.1, $^1J_{C\text{-}N}$ = 1.3, C4), 161.3 (d, $^3J_{C\text{-}N}$ = 3.6, C2), 156.2 (d, $^3J_{C\text{-}N}$ = 19.3, C6), 152.5 (C1'), 129.5 (C4'), 129.4 (d, $^3J_{C\text{-}N}$ = 2.0, C3'), 121.7 ($^2J_{C\text{-}N}$ = 3.7, C2'), 118.8 (dd, $^2J_{C\text{-}1'N}$ = 4.1, $^2J_{C\text{-}4N}$ = 1.2, C5); ^{15}N NMR (DMSO-d_6, 298.5 K): 96.4 (d, $^{2h}J_{N\text{-}N}$ = 5.6, N4), 444.8 (d, $^{2h}J_{N\text{-}N}$ = 5.6, N1'); ESI MS, *m/z* (%): 251.1 [M + H]$^+$; HRMS (ESI) calcd for $C_{10}H_{10}ClN_4{}^{15}N_2$ [M + H]$^+$ 251.0591, found 251.0591.

General procedure C. Methylamine (3 eq, 33 % ethanolic solution) was added to the solution of compound **1** in iPrOH (15 mL) and the reaction mixture was heated under MW conditions at 150 °C. Water (30 mL) was added and the solution was extracted wit EtOAc (3 x 20 mL). Organic layers were collected, dried over $MgSO_4$ and filtered. The solution was evaporated under vacuum. Product was purified by reversed-phase flash chromatography (0-100 % MeOH in water).

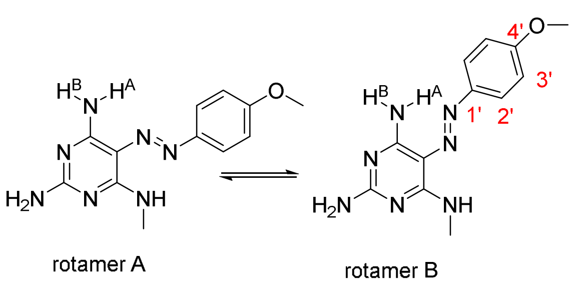

5-((4-Methoxyphenyl)diazenyl)-N^4-methylpyrimidine-2,4,6-triamine (**2a**). Treatment of **1a** (200 mg, 0.7 mmol) with methylamine (0.1 mL, 2.1 mmol) for 30 min by procedure C gave **2a** (70 mg, 37 %) as a yellow solid, m. p. 193–195 °C. ^{1}H NMR (DMF-d_7, 230 K): 10.43 (1H, q, $J_{NH\text{-}CH3}$ = 4.8, 6-NH, A), 9.76 (1H, d, J_{GEM} = 4.5, 4-NH^{A}, B), 7.88-7.95 (5H, m, H2’, A and B, 4-NH^{b}, B), 7.80 (1H, q, $J_{NH\text{-}CH3}$ = 4.6, 6-NH, B), 7.54 and 7.34 (2H, 4-NH$_2$, A), 6.98-7.10 (8H, m, 2-NH$_2$, A and B, H3’, A and B), 3.84 (5H, s, OCH$_3$, A and B), 2.99 (3H, d, $J_{CH3\text{-}NH}$ = 4.8, NH**CH$_3$**, A), 2.97 (3H, d, $J_{CH3\text{-}NH}$ = 4.6, NH**CH$_3$**, B); ^{13}C NMR (DMF-d_7, 230 K): 164.6 (C4, A), 163.8 (C2,A and C2, B), 162.8 (C6, B), 159.2 (C4’, B), 159.1 (C4’, A), 156.6 (C6, A), 155.4 (C4, B), 147.8 (C1’, B), 147.5 (C1’, A), 122.6 (C2’, A and B), 114.1 (C3’, A and B), 109.7 (C5, A and B), 55.3 (OCH$_3$, A and B), 27.4 (NHCH$_3$, B), 26.5 (NHCH$_3$, A); ESI MS, *m/z* (%): 274.1 [M + H]$^+$; HRMS (ESI) calcd for $C_{12}H_{16}N_7O$ [M + H]$^+$ 274.1411, found 274.1411.

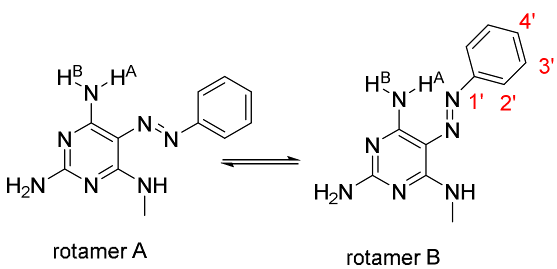

N^{4}-Methyl-5-(phenyldiazenyl)pyrimidine-2,4,6-triamine (**2b**). Treatment of **1b** (75 mg, 0.3 mmol) with methylamine (0.03 mL, 0.9 mmol) for 30 min by procedure C gave **2b** (20 mg, 27 %) as a yellow solid, m. p. 183–187 °C. ^{1}H NMR (DMF-d_7, 230 K): 10.60 (1H, q, $J_{NH,CH3}$= 4.9, 6-NH^{a}), 9.92 (1H, d, J_{GEM}= 5.3, 4-NH^{a}, B), 8.02 (1H, d, J_{GEM}= 5.3, 4-NH^{b}, B), 7.60-7.87 (5H, m, H2’, A and B) 7.63 (1H, s, 4-NH^{a}, A), 7.42 (4H, m, H3’, A and B), 7.30 (1H, s, 4-NH^{b}, A), 7.28-7.22 (2H, m, H4’, A and B), 7.21-7.10 (4H, m, 2-NH$_2$, A and B), 3.02 (3H, d, J_{CH3NH} = 4.8, NH-**CH$_3$**, A), 2.99 (3H, d, J_{CH3NH} = 4.8, NH-**CH$_3$**, B); ^{13}C NMR (DMF-d_7, 230 K): 165.6 (C4, A), 164.8 (C2, A and B), 163.6 (C6, B), 156.4 (C6, A), 156.4 (C4, B), 154.3 (C1’, B), 154.2 (C1’, A), 129.9 (C3’ and C5’, B), 129.8 (C3’ and C5’, A), 127.8 (C4’, B), 127.7 (C4’, A), 121.9 (C2’ and C6’, A and B), 111.1 (C5, A and B), 28.1 (CH$_3$NH, B), 27.1 (CH$_3$NH, A); ^{15}N NMR (DMF-d_7, 230 K): 399.2

(N1’, B), 391.8 (N1’, A), 92.0 (N4, B), 89.2 (N6, A), 78.6 (N4, A), 73.4 (N6, B); ESI MS, *m/z* (%): 244.1 $[M + H]^+$; HRMS (ESI) calcd for $C_{11}H_{14}N_7$ $[M + H]^+$ 244.1305, found 244.1305.

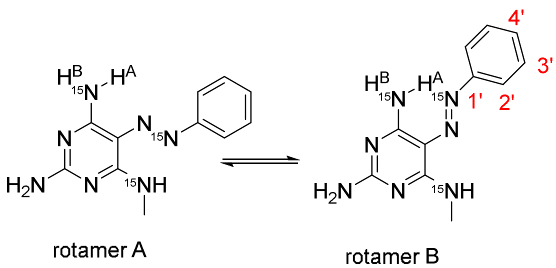

N^4-Methyl-5-(phenyldiazenyl-2-^{15}N)pyrimidine-2,4,6-triamine-N^4-$^{15}N^2$ (**2b-^{15}N$_3$**). Treatment of **1b-^{15}N$_2$** (200 mg, 0.8 mmol) with methylamine-^{15}N hydrochloride (109 mg, 1.6 mmol) for 1 h by procedure C gave **2b-^{15}N$_3$** (40 mg, 20 %) as a yellow solid, m. p. 178–181 °C. ^{1}H NMR (DMF-d_7, 230 K): 10.60 (1H, dp, $J_{H\text{-}N}$ = 92.9, $J_{NH\text{-}CH3}$ = 4.7, $^{1h}J_{H\text{-}N}$ = 4.0, 6-NH, A), 9.92 (1H, dm, $J_{H\text{-}N}$ = 89.0, 4-NH^a, B), 8.13-7.87 (5H, m, H2’, A and B, 4-NH^B, B), 7.88 (1H, dq, $J_{H\text{-}N}$ = 95.3, $J_{NH\text{-}CH3}$ = 4.8, 6-NH, B), 7.61 (1H, dd, $J_{H\text{-}N}$ = 91.5, J_{GEM} = 2.5, 4-NH^A, A) 7.46-7.22 (6H, m, H3’, A and B, H4’, A and B, 4-NH^B, A), 7.18-7.08 (4H, m, 2-NH$_2$, A and B), 3.02 (3H, dd, $J_{CH3\text{-}NH}$ = 4.9, $J_{CH3\text{-}N}$ = 1.2, **CH$_3$**NH, A), 2.99 (2.1 dd, $J_{CH3\text{-}NH}$ = 4.9, $J_{CH3\text{-}N}$ = 1.2, **CH$_3$**NH, B); ^{13}C NMR (DMF-d_7, 234 K): 165.6 (d, $J_{C\text{-}N}$ = 21.1, C4, A), 164.8 (t, $^3J_{C\text{-}6N}$ = ^3JC$_{\text{-}4N}$ = 3.4, C2, A and B), 163.6 (m, C6, B), 156.4 (d, $J_{C\text{-}N}$ = 18.3, C6, A), 156.3 (d, $J_{C\text{-}N}$ = 18.0, C4, B), 154.4 (C1’, B), 154.2 (C1’, A), 129.9 (C3’, B), 129.9 (C3’, A), 127.8 (C4’, B), 127.7 (C4’, A), 121.9 (d, $^2J_{C\text{-}N}$ = 3.5, C2’, A), 111.1 (m, C5, A and B), 28.1 (d, $J_{C\text{-}N}$ = 11.9, CH$_3$NH, B), 27.1 (d, $J_{C\text{-}N}$ = 10.9, CH$_3$NH, A); ^{15}N NMR (DMF-d_7, 230 K): 99.16 (d, $^2J_{N\text{-}N}$ = 6.3, N1’, B), 91.87 (d, $^2J_{N\text{-}N}$ = 7.5, N1’, A), 92.03 (td, $J_{N.Ha}$ = $J_{N\text{-}Hb}$ = 90.8, $^{2h}J_{N\text{-}N}$ = 6.3, N4, B), 89.22 (t, $J_{N\text{-}H}$ = 91.1, N4, A), 73.45 (d, $J_{N\text{-}H}$ = 95.1, N6, B); ESI MS, *m/z* (%): 247.2 $[M + H]^+$; HRMS (ESI) calcd for $C_{11}H_{14}N_4{}^{15}N_3$ $[M + H]^+$ 247.1216, found 247.1217.

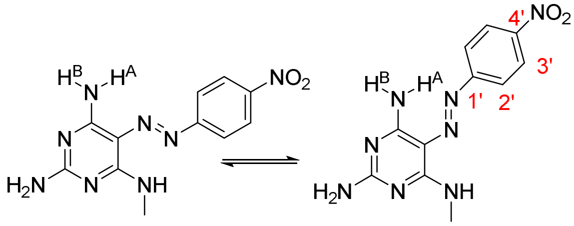

rotamer A rotamer B

N^4-Methyl-5-((4-nitrophenyl)diazenyl)pyrimidine-2,4,6-triamine (**2c**). Treatment of **1c** (200 mg, 0.7 mmol) with methylamine (0.08 mL, 2.1 mmol) for 10 min by procedure C gave **2c** (80 mg, 40 %) as a red solid, m. p. > 300 °C. ^{1}H NMR (DMSO-d_6): 10.69 (1H, bs, 6-NH, A), 9.87 (1H, bs, 4-NH^A, B), 8.18-8.22 (4H, m, H3', A and H3', B), 7.93-8.03 (4H, m, H2', A and H2', B), 7.84 (1H, bs, 4-NH^B, B), 7.73 (1H, bs, 6-NH, B), 7.36 and 7.04 (2-NH$_2$, A), 2.99 (3H, bs, **CH$_3$**NH, A), 2.94 (3H, bs, (**CH$_3$**NH, B); ^{13}C NMR (DMSO-d$_6$): 164.6 (C4, A), 163.9-164.0 (m, C2, A and B), 162.6 (C6, B), 158.1 (C1', A and B), 155.5 (C4, B), 155.4 (C6, A), 144.3 (C4', A and B), 124.9 (C3', A and B), 121.1 (C2', A and B), 112.7 (C5, A and B), 27.8 (CH$_3$, B), 27.0 (CH$_3$, A); ESI MS, *m/z* (%): 289.1 [M + H]$^+$; HRMS (ESI) calcd for $C_{11}H_{13}N_8O_2$ [M + H]$^+$ 289.1156, found 289.1156.

Acknowledgment

The work has been supported by the Czech Science Foundation (grant no. 15-11223S).

Supporting Information

Synthesis of compound **2d**, additional NMR spectra, additional figures and tables, ^{1}H and ^{13}C spectra of newly prepared compounds, Cartesian coordinates of transition-state structures.

This material can be downloaded free of charge via the internet at http://pubs.acs.org.

References

1. Hobza, P.; Havlas, Z. Blue-Shifting Hydrogen Bonds. *Chem. Rev.* **2000,** *100*, 4253-4264.

2. Grabowski, S. J. What Is the Covalency of Hydrogen Bonding? *Chem. Rev.* **2011,** *111*, 2597-2625.

3. Grzesiek, S.; Cordier, F.; Jaravine, V.; Barfield, M. Insights into Biomolecular Hydrogen Bonds from Hydrogen Bond Scalar Couplings. *Prog. Nucl. Magn. Reson. Spectrosc.* **2004,** *45*, 275-300.

4. Kuhn, B.; Mohr, P.; Stahl, M. Intramolecular Hydrogen Bonding in Medicinal Chemistry. *J. Med. Chem.* **2010,** *53*, 2601-2611.

5. Furet, P.; Caravatti, G.; Guagnano, V.; Lang, M.; Meyer, T.; Schoepfer, J. Entry into a New Class of Protein Kinase Inhibitors by Pseudo Ring Design. *Bioorg. Med. Chem. Lett.* **2008,** *18*, 897-900.

6. Hodge, C. N.; Pierce, J. A Diazine Heterocycle Replaces a 6-Membered Hydrogen-Bonded Array in the Active-Site of Scytalone Dehydratase. *Bioorg. Med. Chem. Lett.* **1993,** *3*, 1605-1608.

7. Furet, P.; Bold, G.; Hofmann, F.; Manley, P.; Meyer, T.; Altmann, K. H. Identification of a New Chemical Class of Potent Angiogenesis Inhibitors Based on Conformational Considerations and Database Searching. *Bioorg. Med. Chem. Lett.* **2003,** *13*, 2967-2971.

8. Menear, K. A.; Adcock, C.; Alonso, F. C.; Blackburn, K.; Copsey, L.; Drzewiecki, J.; Fundo, A.; Le Gall, A.; Gomez, S.; Javaid, H.; Lence, C. F.; Martin, N. M. B.; Mydlowski, C.; Smith, G. C. M. Novel Alkoxybenzamide Inhibitors of Poly(ADP-Ribose) Polymerase. *Bioorg. Med. Chem. Lett.* **2008,** *18*, 3942-3945.

9. Lord, A. M.; Mahon, M. F.; Lloyd, M. D.; Threadgill, M. D. Design, Synthesis, and Evaluation in Vitro of Quinoline-8-Carboxamides, a New Class of Poly(Adenosine-Diphosphate-Ribose)Polymerase-1 (PARP-1) Inhibitor. *J. Med. Chem.* **2009,** *52*, 868-877.

10. Osmialowski, B.; Kolehmainen, E.; Kowalska, M. 2-Acylamino-6-Pyridones: Breaking of an Intramolecular Hydrogen Bond by Self-Association and Complexation with Double and Triple Hydrogen Bonding Counterparts. Uncommon Steric Effect on Intermolecular Interactions. *J. Org. Chem.* **2012,** *77*, 1653-1662.

11. Procházková, E.; Čechová, L.; Janeba, Z.; Dračínský, M. A Switchable Intramolecular Hydrogen Bond in Polysubstituted 5-Nitrosopyrimidines. *J. Org. Chem.* **2013,** *78*, 10121-10133.

12. Olivella, M.; Marchal, A.; Nogueras, M.; Melguizo, M.; Lima, B.; Tapia, A.; Feresin, G. E.; Parravicini, O.; Giannini, F.; Andujar, S. A.; Cobo, J.; Enriz, R. D. A New Series of Antibacterial Nitrosopyrimidines: Synthesis and Structure-Activity Relationship. *Arch. Pharm.* **2015,** *348*, 68-80.

13. Illán-Cabeza, N. A.; García-García, A. R.; Moreno-Carretero, M. N. Theoretical Investigations on the Structure and Relative Stabilities of the Tautomeric Forms of 6-Amino-5-Nitrosouracil and Violuric Acid Derivatives (PM3-Cosmo Calculation). *Comput. Theor. Chem.* **2011,** *964*, 83-90.

14. Illán-Cabeza, N. A.; García-García, A. R.; Moreno-Carretero, M. N. Complexes with 6-Amino-5-Nitroso-2-Thiouracil and Violuric Acid Derivatives Containing the *fac*-$Re^{I}(CO)_3$ Core: Synthesis, XRD Structural and Photoluminescence Characterization. *Inorg. Chim. Acta* **2011,** *366*, 262-267.

15. Čechová, L.; Procházková, E.; Císařová, I.; Dračínský, M.; Janeba, Z. Separation of Planar Rotamers through Intramolecular Hydrogen Bonding in Polysubstituted 5-Nitrosopyrimidines. *Chem. Commun.* **2014,** *50*, 14892-14895.

16. Bolvig, S.; Hansen, P. E. Isotope Effects on Chemical Shifts as an Analytical Tool in Structural Studies of Intramolecular Hydrogen Bonded Compounds. *Curr. Org. Chem.* **2000,** *4*, 19-54.

17. Sobczyk, L.; Grabowski, S. J.; Krygowski, T. M. Interrelation between H-Bond and Pi-Electron Delocalization. *Chem. Rev.* **2005,** *105*, 3513-3560.

18. Lyssenko, K. A.; Antipin, M. V. The Nature and Energy Characteristics of Intramolecular Hydrogen Bonds in Crystals. *Russ. Chem. Bull.* **2006,** *55*, 1-15.

19. Dračínský, M.; Čechová, L.; Hodgkinson, P.; Procházková, E.; Janeba, Z. Resonance-Assisted Stabilisation of Hydrogen Bonds Probed by NMR Spectroscopy and Path Integral Molecular Dynamics. *Chem. Commun.* **2015,** *51*, 13986-13989.

20. Procházková, E.; Čechová, L.; Tarábek, J.; Janeba, Z.; Dračínský, M. Tunable Push-Pull Interactions in 5-Nitrosopyrimidines. *J. Org. Chem.* **2016,** *81*, 3780-3789.

21. Dračínský, M. The Chemical Bond: The Perspective of NMR Spectroscopy. *Annu. Rep. NMR Spectrosc.* **2017,** *90*, 1-40.

22. Löhr, F.; Mayhew, S. G.; Ruterjans, H. Detection of Scalar Couplings across NH···OP and OH··· OP Hydrogen Bonds in a Flavoprotein. *J. Am. Chem. Soc.* **2000,** *122*, 9289-9295.

23. Dingley, A. J.; Grzesiek, S. Direct Observation of Hydrogen Bonds in Nucleic Acid Base Pairs by Internucleotide $^{2}J_{NN}$ Couplings. *J. Am. Chem. Soc.* **1998,** *120*, 8293-8297.

24. Pervushin, K.; Ono, A.; Fernandez, C.; Szyperski, T.; Kainosho, M.; Wüthrich, K. NMR Scaler Couplings across Watson-Crick Base Pair Hydrogen Bonds in DNA Observed by Transverse Relaxation Optimized Spectroscopy. *Proc. Natl. Acad. Sci. USA* **1998,** *95*, 14147-14151.

25. Czernek, J.; Brüschweiler, R. Geometric Dependence of $^{3h}J(^{31}P–^{15}N)$ and $^{2h}J(^{31}P–^{1}H)$ Scalar Couplings in Protein-Nucleotide Complexes. *J. Am. Chem. Soc.* **2001,** *123*, 11079-11080.

26. Alkorta, I.; Elguero, J.; Denisov, G. S. A Review with Comprehensive Data on Experimental Indirect Scalar NMR Spin-Spin Coupling Constants across Hydrogen Bonds. *Magn. Reson. Chem.* **2008,** *46*, 599-624.

27. Afonin, A. V.; Vashchenko, A. V. Theoretical Study of Bifurcated Hydrogen Bonding Effects on the ^{1}J(N,H), ^{1h}J(N,H), ^{2h}J(N,N) Couplings and ^{1}H, ^{15}N Shieldings in Model Pyrroles. *Magn. Reson. Chem.* **2010,** *48*, 309-317.

28. Freeman, N. S.; Moore, C. E.; Wilhelmsson, L. M.; Tor, Y. Chromophoric Nucleoside Analogues: Synthesis and Characterization of 6-Aminouracil-Based Nucleodyes. *J. Org. Chem.* **2016,** *81*, 4530-4539.

29. Procházková, E.; Jansa, P.; Dračínský, M.; Holý, A.; Mertlíková-Kaiserová, H. Determination of the Antioxidative Activity of Substituted 5-Aminopyrimidines. *Free Radical Res.* **2012,** *46*, 61-67.

30. Puntoriero, F.; Ceroni, P.; Balzani, V.; Bergamini, G.; Vogtle, F. Photoswitchable Dendritic Hosts: A Dendrimer with Peripheral Azobenzene Groups. *J. Am. Chem. Soc.* **2007,** *129*, 10714-10719.

31. Ferri, V.; Elbing, M.; Pace, G.; Dickey, M. D.; Zharnikov, M.; Samori, P.; Mayor, M.; Rampi, M. A. Light-Powered Electrical Switch Based on Cargo-Lifting Azobenzene Monolayers. *Angew. Chem. Int. Ed.* **2008,** *47*, 3407-3409.

32. Banghart, M. R.; Mourot, A.; Fortin, D. L.; Yao, J. Z.; Kramer, R. H.; Trauner, D. Photochromic Blockers of Voltage-Gated Potassium Channels. *Angew. Chem. Int. Ed.* **2009,** *48*, 9097-9101.

33. Banghart, M.; Borges, K.; Isacoff, E.; Trauner, D.; Kramer, R. H. Light-Activated Ion Channels for Remote Control of Neuronal Firing. *Nat. Neurosci.* **2004,** *7*, 1381-1386.

34. Muraoka, T.; Kinbara, K.; Aida, T. Mechanical Twisting of a Guest by a Photoresponsive Host. *Nature* **2006,** *440*, 512-515.

35. Gorostiza, P.; Isacoff, E. Y. Optical Switches for Remote and Noninvasive Control of Cell Signaling. *Science* **2008,** *322*, 395-399.

36. Stoll, R. S.; Peters, M. V.; Kuhn, A.; Heiles, S.; Goddard, R.; Bühl, M.; Thiele, C. M.; Hecht, S. Photoswitchable Catalysts: Correlating Structure and Conformational Dynamics with Reactivity by a Combined Experimental and Computational Approach. *J. Am. Chem. Soc.* **2009,** *131*, 357-367.

37. Koshima, H.; Ojima, N.; Uchimoto, H. Mechanical Motion of Azobenzene Crystals Upon Photoirradiation. *J. Am. Chem. Soc.* **2009,** *131*, 6890-6891.

38. Khan, A.; Hecht, S. Towards Photocontrol over the Helix-Coil Transition in Foldamers: Synthesis and Photoresponsive Behavior of Azobenzene-Core Amphiphilic Oligo(Meta-Phenylene Ethynylene)s. *Chem. Eur. J.* **2006,** *12*, 4764-4774.

39. Mathews, M.; Tamaoki, N. Planar Chiral Azobenzenophanes as Chiroptic Switches for Photon Mode Reversible Reflection Color Control in Induced Chiral Nematic Liquid Crystals. *J. Am. Chem. Soc.* **2008,** *130*, 11409-11416.

40. Bandara, H. M. D.; Burdette, S. C. Photoisomerization in Different Classes of Azobenzene. *Chem. Soc. Rev.* **2012,** *41*, 1809-1825.

41. Müller, K.; Knebel, A.; Zhao, F. L.; Bleger, D.; Caro, J.; Heinke, L. Switching Thin Films of Azobenzene-Containing Metal-Organic Frameworks with Visible Light. *Chem. Eur. J.* **2017,** *23*, 5434-5438.

42. Alaasar, M.; Prehm, M.; Poppe, S.; Tschierske, C. Development of Polar Order by Liquid-Crystal Self-Assembly of Weakly Bent Molecules. *Chem. Eur. J.* **2017,** *23*, 5541-5556.

43. Lubbe, A. S.; Szymanski, W.; Feringa, B. L. Recent Developments in Reversible Photoregulation of Oligonucleotide Structure and Function. *Chem. Soc. Rev.* **2017,** *46*, 1052-1079.

44. Wang, D. S.; Wagner, M.; Saydjari, A. K.; Mueller, J.; Winzen, S.; Butt, H. J.; Wu, S. A Photoresponsive Orthogonal Supramolecular Complex Based on Host-Guest Interactions. *Chem. Eur. J.* **2017,** *23*, 2628-2634.

45. Bisoyi, H. K.; Li, Q. Light -Driven Liquid Crystalline Materials: From Photo -Induced Phase Transitions and Property Modulations to Applications. *Chem. Rev.* **2016,** *116*, 15089-15166.

46. Dingley, A. J.; Masse, J. E.; Peterson, R. D.; Barfield, M.; Feigon, J.; Grzesiek, S. Internucleotide Scalar Couplings across Hydrogen Bonds in Watson-Crickand Hoogsteen Base Pairs of a DNA Triplex. *J. Am. Chem. Soc.* **1999,** *121*, 6019-6027.

47. Dračínský, M.; Hodgkinson, P. Effects of Quantum Nuclear Delocalisation on NMR Parameters from Path Integral Molecular Dynamics. *Chem. Eur. J.* **2014,** *20*, 2201-2207.

48. Dračínský, M.; Bouř, P.; Hodgkinson, P. Temperature Dependence of NMR Parameters Calculated from Path Integral Molecular Dynamics Simulations. *J. Chem. Theory Comput.* **2016,** *12*, 968-973.

49. Luduena, G. A.; Wegner, M.; Bjålie, L.; Sebastiani, D. Local Disorder in Hydrogen Storage Compounds: The Case of Lithium Amide/Imide. *ChemPhysChem* **2010,** *11*, 2353-2360.

50. Shiga, M.; Suzuki, K.; Tachikawa, M. The Chemical Shift of Deprotonated Water Dimer: Ab Initio Path Integral Simulation. *J. Chem. Phys.* **2010,** *132*, 114104.

51. Li, X. Z.; Walker, B.; Michaelides, A. Quantum Nature of the Hydrogen Bond. *Proc. Nat. Acad. Sci. USA* **2011,** *108*, 6369-6373.

52. Taylor, R.; Kennard, O.; Versichel, W. The Geometry of the N-H ... O=C Hydrogen-Bond .3. Hydrogen-Bond Distances and Angles. *Acta Crystallogr. B* **1984,** *40*, 280-288.

53. Becke, A. D. Density-Functional Thermochemistry 3. The Role of Exact Exchange. *J. Chem. Phys.* **1993,** *98*, 5648-5652.

54. Lee, C. T.; Yang, W. T.; Parr, R. G. Development of the Colle-Salvetti Correlation-Energy Formula into a Functional of the Electron-Density. *Phys. Rev. B* **1988,** *37*, 785-789.

55. Barone, V.; Cossi, M. Quantum Calculation of Molecular Energies and Energy Gradients in Solution by a Conductor Solvent Model. *J. Phys. Chem. A* **1998,** *102*, 1995-2001.

56. Cossi, M.; Rega, N.; Scalmani, G.; Barone, V. Energies, Structures, and Electronic Properties of Molecules in Solution with the C-PCM Solvation Model. *J. Comput. Chem.* **2003,** *24*, 669-681.

57. Frisch, M. J.; Trucks, G. W.; Schlegel, H. B.; Scuseria, G. E.; Robb, M. A.; Cheeseman, J. R.; Scalmani, G.; Barone, V.; Mennucci, B.; Petersson, G. A.; Nakatsuji, H.; Caricato, X.; Li, X.; Hratchian, H. P.; Izmaylov, A. F.; Bloino, J.; Zheng, G.; Sonnenberg, J. L.; Hada, M.; Ehara, M.; Toyota, K.; Fukuda, R.; Hasegawa, J.; Ishida, M.; Nakajima, T.; Honda, Y.; Kitao, O.; Nakai, H.; Vreven, T.; Montgomery, J., J. A.; Peralta, J. E.; Ogliaro, F.; Bearpark, M.; Heyd, J. J.; Brothers, E.; Kudin, K. N.; Staroverov, V. N.; Kobayashi, R.; Normand, J.; Raghavachari, K.; Rendell, A.; Burant, J. C.; Iyengar, S. S.; Tomasi, J.; Cossi, M.; Rega, N.; Millam, J. M.; Klene, M.; Knox, J. E.; Cross, J. B.; Bakken, V.; Adamo, C.; Jaramillo, J.; Gomperts, R.; Stratmann, R. E.; Yazyev, O.; Austin, A. J.; Cammi, R.; Pomelli, C.; Ochterski, J. W.; Martin, R. L.; Morokuma, K.; Zakrzewski, V. G.; Voth, G. A.; Salvador, P.; Dannenberg, J. J.; Dapprich, S.; Daniels, A. D.; Farkas, O.; Foresman, J. B.; Ortiz, J. V.; Cioslowski, J.; Fox, D. J. *Gaussian 09, Revision A.02*, Gaussian, Inc.: Wallingford CT, 2009.

58. Peng, C.; Ayala, P. Y.; Schlegel, H. B.; Frisch, M. J. Using Redundant Internal Coordinates to Optimize Equilibrium Geometries and Transition States. *J. Comput. Chem.* **1996,** *17*, 49-56.

59. Peng, C.; Schlegel, H. B. Combining Synchronous Transit and Quasi-Newton Methods for Finding Transition States. *Israel J. Chem.* **1994,** *33*, 449-454.

60. Clark, S. J.; Segall, M. D.; Pickard, C. J.; Hasnip, P. J.; Probert, M. J.; Refson, K.; Payne, M. C. First Principles Methods Using CASTEP. *Z. Kristallogr.* **2005,** *220*, 567-570.

61. Vanderbilt, D. Soft Self-Consistent Pseudopotentials in a Generalized Eigenvalue Formalism. *Phys. Rev. B* **1990,** *41*, 7892-7895.

62. Monkhorst, H. J.; Pack, J. D. Special Points for Brillouin-Zone Integrations. *Phys. Rev. B* **1976,** *13*, 5188-5192.

63. Perdew, J. P.; Burke, K.; Ernzerhof, M. Generalized Gradient Approximation Made Simple. *Phys. Rev. Lett.* **1996,** *77*, 3865-3868.